Received: 15 January 2021 | Revised: 21 July 2021 | Accepted: 12 August 2021

DOI: 10.1002/joc.7356

International Journal of Climatology RMetS

RESEARCH ARTICLE

A newly developed South American Mapping of Temperature with estimated lapse rate corrections

José Roberto Rozante | **Enver Ramirez** | **Alex de Almeida Fernandes**

Center for Weather Forecast and Climate Studies, National Institute for Space Research, Cachoeira Paulista, Brazil

Correspondence
José Roberto Rozante, Center for Weather Forecast and Climate Studies, National Institute for Space Research, Rodovia Presidente Dutra, Km 40, SP-RJ-CEP: 12630-000, Cachoeira Paulista, SP, Brazil.
Email: roberto.rozante@inpe.br

Abstract

In the present work a recently developed product, the South American Mapping of Temperature (SAMeT), is presented. SAMeT minimizes certain deficiencies associated with both the eventual lack of observations and incorporates temperature corrections due to elevation or lapse rate of temperature (LRT) considerations. SAMeT is based on combinations of observed 2-m temperatures and ERA5 reanalysis, as well as LRTs values computed from maximum (Tmax) and minimum (Tmin) temperatures. The LRT were computed using a simple linear regression on a 40-year ERA5 reanalysis dataset and a digital elevation model dataset from Global Digital Elevation (GTOPO30). It was obtained that the computed LRT is consistently smaller than the standard LRT for all the seasons and studied regions. The South American territory was divided into four subdomains and the evaluation performed via a cross validation. This methodology consists in removing 90% of the observations to form OBS90 and generate the SAMeT fields. The remaining 10% (OBS10) is used for validation purposes. An additional dataset, hereafter referred to as OBS90i, is obtained using Kriging interpolation of OBS90 along with GTOPO30 and temperature adjustment by a standard LRT ($-6.5^{\circ}C \cdot km^{-1}$). The evaluation period was from January 2011 to December 2013. Thus by using the standard LRT, a systematic negative bias for the temperature is obtained. On the other hand, ERA5 displays underestimation for Tmax and overestimation for Tmin. Furthermore, in comparative terms ERA5 displays the larger errors; thus, it is suggested that a bias remotion is important for any application involving these data. The systematic application of computed values for LRT in addition to a combination between observations and ERA5 data allows SAMeT to generate fields with smaller errors compared to observations than ERA5 while keeping spatial correlations. Thus, the present product brings an innovation to the temperature space fields for the South American region.

KEYWORDS

lapse rate, SAMeT, South American, temperature

1 | INTRODUCTION

Temperature is one of the most important meteorological variables for diverse activities ranging from management of water resources, agrometeorological applications and climate studies. It also serves as initial and boundary conditions for numerical models. Temperature is measured by meteorological stations at a height of 2 m above the surface (T2m) and their representivity is limited to surrounding areas of the point in which data are collected, at best, being valid within a radius of 100 km (WMO, 2010). The knowledge of their regular space–time distribution can be used for several applications, such as hydrology (Piani *et al*., 2010; Tobin *et al*., 2011), ecology (Régnière and Sharov, 1999; Monestiez *et al*., 2001), agriculture (Schlenker and Roberts, 2009; Zhao *et al*., 2017), energy (Jaglom *et al*., 2014; Scapin *et al*., 2016), among others.

Regularly spaced products for T2m derived from randomly distributed weather stations are obtained by taking the observations to a reference vertical level, performing the interpolation there and after that returned to the corresponding height in the regularly spaced grid by correcting information through both the lapse rate of temperature and topographic information. However, we have noted that for regions with scarce number of stations the quality of the interpolated field (by solely using stations) may not satisfactorily represent the real conditions and additional information is needed, like for example those provided from a reanalysis. Of particular interest are the mountainous regions with a high-altitude variability (i.e., not a plateau) that lead to high spatial temperature variability (Córdova *et al*., 2016); the presence of topography over a determined region contributes to the spatial variability. Thus, the main uncertainties of the interpolated T2m products could be associated to the lack of observed data and to the representativeness of the lapse rate of temperature (LRT) used for the interpolation processes (Dodson and Marks, 1997; Jobst *et al*., 2017). Therefore, uncertainties in the interpolated field can be associated with both the lack of a necessary correction due to the temperature decrease with height (LRT) and to the spatial data scarcity (Dodson and Marks, 1997; Jobst *et al*., 2017).

Many authors have worked around the limitations related to the LRT by applying horizontal interpolation methods that take into account the altitude of the region to which data are being interpolated. Although there is evidence that the LRT can vary over space and time, many authors are inclined to use the international standard atmosphere (ISA) with a temperature lapse rate of $-6.5°C·km^{-1}$ in their interpolation methods (Maurer *et al*., 2002; Hamlet and Lettenmaier, 2005; Arnold *et al*., 2006). However, more judicious studies prefer to estimate the LRT values, since the use of constant LRT may not be a fair representative of the atmosphere at a given location, such as valleys, where the thermal inversion can significantly change the LRT. One of such studies by Rolland (Rolland, 2003) has shown the temporal and spatial variability of the LRT for a mountainous region of the United States (using observations and numerical models). Rolland has shown that the constant LRT approach ($-6.5°C·km^{-1}$) has proven to be not a close estimate, since computed LRT values were substantially lower (between −3.9 and $-5.2°C·km^{-1}$) than the constant value of $-6.5°C·km^{-1}$. Similar considerations have also been found over the Tianshan Mountains in China (Shen *et al*., 2016), Canadian Arctic glaciers (Marshall *et al*., 2007; Gardner *et al*., 2009), Arizona's semiarid (Harlow *et al*., 2004) and Italian Alps (Rolland, 2003).

Another limitation of the interpolated fields is associated with the scarcity of observed data over mountains, forests, deserts and oceans, and according to Vizuete *et al*. (2002) the accuracy of the interpolated fields may vary significantly between the different interpolation methods depending on the spatial distribution of the dataset. In this sense, the choice of the spatial interpolation method is of paramount importance in regions where data distribution is sparse. Thus, in order to minimize the interpolation errors associated with the lack of observations, data from numerical models (Fuentes and Raftery, 2005; Kann *et al*., 2011), reanalysis (Essou *et al*., 2017; Chen *et al*., 2019) and satellite estimates (Rozante *et al*., 2010; 2020) have been combined to surface observations in order to produce a more coherent meteorological fields. Many studies have been concentrated to address precipitation products over different regions such as South America (Vila *et al*., 2009; Rozante *et al*., 2010; 2020), China (Shuai Han and Shuai Han, 2019), Asia (Jia *et al*., 2013), Ethiopia (Dinku *et al*., 2014), Nigeria (Grimes *et al*., 1999), Australia (Chappell *et al*., 2013), India (Mitra *et al*., 2013), among others. However, relatively less studies with a focus on temperature has been found. Chen *et al*. (2019) combined observed temperature data for China with reanalysis data from the European Center for Medium Range Weather Forecasts (ECMWF) and concluded that interpolated temperature errors increase with altitude and reduces with increasing data density.

The main objective of the present study is to investigate whether the combination of observed T2m and reanalysis corrected through a variable LRT is capable of producing more realistic high resolution (5 km) temperature fields over South America. The resulting product of the combination of observed data, reanalysis and the

correction by the variable LRT, henceforth called South America Mapping of Temperature (SAMeT), will be generated and made operationally available from January 2000 to the present.

2 | DATA AND METHODOLOGY

2.1 | Area of study

South America is the fourth largest contiguous land mass (Alvarez-Varas *et al.*, 2016), stretching from the Gulf of Darién in the northwest to the archipelago of Tierra del Fuego to the south. The southernmost latitude is 55°S, while the northernmost is at 12°N. It is bathed by the Caribbean Sea (to the north), Atlantic Ocean to the east and the Pacific Ocean to the west; all of them have a strong influence on the circulation characteristics of the continent (Satyamurty *et al.*, 1998). Another important and distinctive geographical feature of the continent is the presence of the Andes, a steep and relatively narrow mountain range that extends, meridionally (about 7,000 km), across the western part of the continent (Figure 1b). The Andes is the longest surface mountain chain and the second tallest surface chain of mountains on earth, reaching almost 7,000 m, playing important roles on the flow over South America including the low level jets, and consequently affecting the transport of moisture from the Amazon to the subtropical regions of the continent (Vera *et al.*, 2006; Insel *et al.*, 2010). Another important feature of South America is the Amazon forest, occupying about 35% of the total continental area and 65% of the tropical area. South America also contains some of the driest places in the world, including

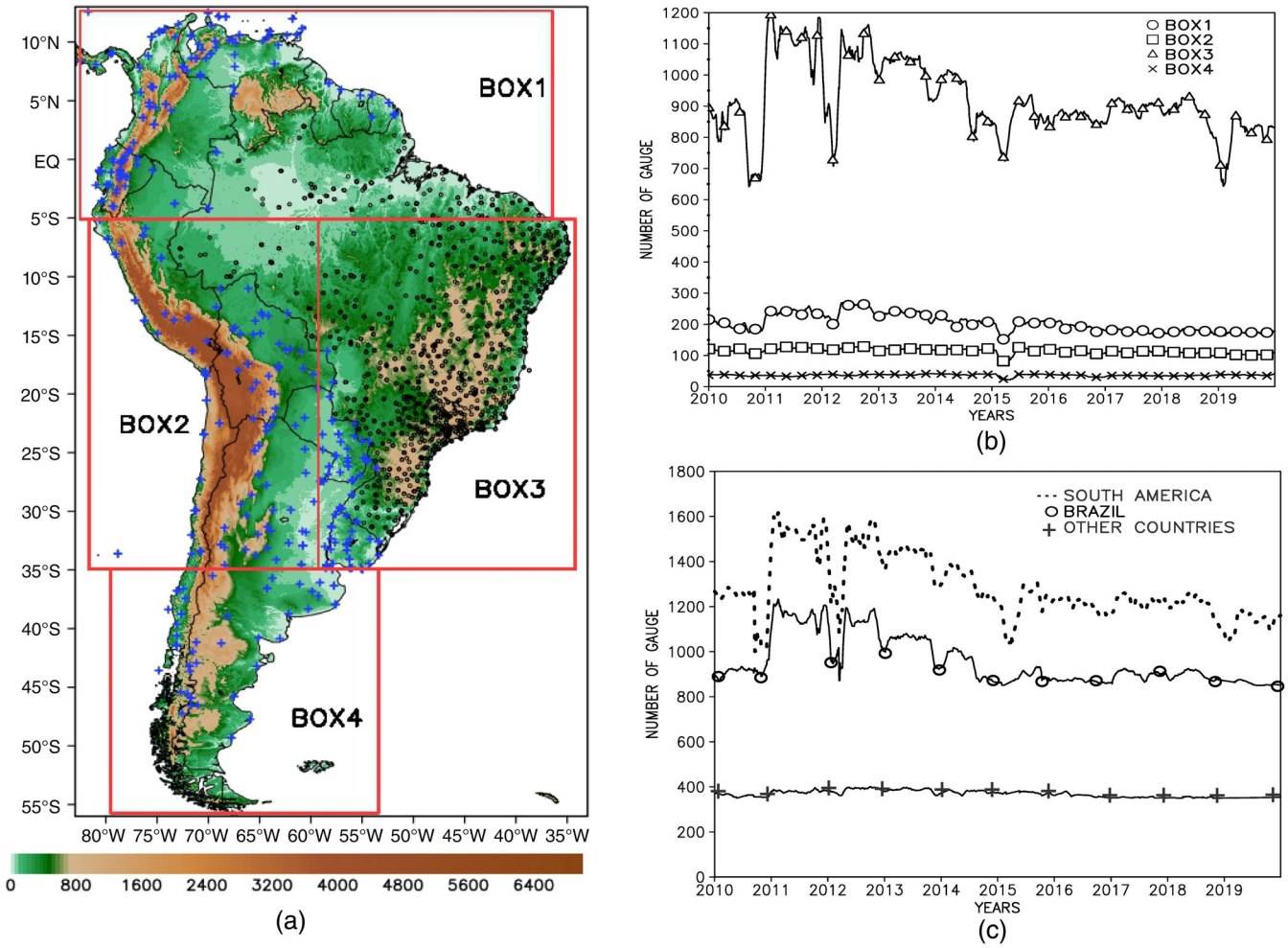

FIGURE 1 A map for the space distribution of the gauge stations (dots for Brazil and crosses for other countries) on top of the GTOPO30 elevation map (shaded) along with the square boxes used to delimitate the computation of the LRT (a); time evolution of the 15-day running mean of the number of observations for each defined box (b); and time evolution of the 15-day running mean of the number of observations for Brazil (open circle), other countries (crosses) and all of South America (dotted) (c) [Colour figure can be viewed at wileyonlinelibrary.com]

the hyperarid (<2 mm·year^{-1}) core of the Atacama Desert in northern Chile (Ritter *et al*., 2019). South America can be divided into four distinct climate zones (Garreaud *et al*., 2009): tropical, temperate, dry and cold; distributed according to the relief and other environmental conditions involving intricate sets of processes that are out of the scope of the present study. In general, rainfall is plentiful in most parts of South America, with the exception of the desert areas of Peru and northern Chile, Argentine Patagonia and northeastern Brazil.

The analysis was regionalized by selecting boxes (Figure 1a). The selection was based on practical results. An initial study performed using a unique LRT for the whole South American continent was made. This zeroth order approach produced better metrics when compared to the ERA5 reanalysis. The selection of a unique value of LRT was supported by an EOF analysis performed over monthly data and for variables like maximum (Tmax) and minimum (Tmin) temperatures. To be more specific, the selection is supported by the EOF1 (not shown) that was obtained after the removal of the seasonal cycle and long-term trends. Moreover, when we performed the separation in boxes, we obtained even better results than those using a unique LRT for the whole South American continent. It is worth mentioning, as suggested by the reviewers, that there is still space for improvements by using a more sophisticated clusterization method like *k*-means, fuzzy *c*-means (e.g., Podani, 2005 and references therein), and in fact we have started exploratory research to apply *k*-means. However, some difficulties inherent to the method has been found and to this point we do not have something ready. More details about boxes are given in section 2.2.

2.2 | Observed data

In the present study, the observed data corresponds to the daily maximum temperature (Tmax), daily minimum (Tmin) and elevation data (H). The data come from different sources (data stations) received operationally by the Brazilian Weather Forecast and Climate Studies Center/National Institute for Space Research (CPTEC/INPE). Concerning the sampling frequency, some sources report daily data, as is the case of the Surface Synoptic Observations (SYNOP) from the Global Telecommunications System (GTS), and either Tmax or Tmin are taken directly. For those the other sources such as METeorological Aerodrome Report (METAR), automatic data collection platform (PCDs) and regional meteorological centres that provide hourly time series of temperature, Tmax and Tmin, are obtained from the diurnal cycle of each weather station.

In Figure 1a the data are depicted using black circles and crosses corresponding to data stations that are within Brazil or that correspond to surrounding countries, respectively. The digital elevation (Digital Elevation – Global 30 Arc-Second Elevation or GTOPO30) is also depicted in shaded. This data were obtained through the spatial data access tool (SDAT; ORNL DAAC, 2017) for more information see https://webmap.ornl.gov. Concerning the spatial distribution, we can see that the density of data stations over BOX1 and BOX3 is decreasing from the coastal strip towards the interior of the continent; this behaviour is more prominent to the north of 10°S. It is also possible to be noted that BOX1 and BOX4 are also characterized for having low density of stations. For BOX4 no data to the south of 50°S is reported by any station (Figure 1a).

The amount of daily observations that report T2m for each BOX varies through the years; the trend to decrease is more accentuated for BOX3 for the other boxes the trend is not perceptible (Figure 1b). Most of the observations are located in BOX3 (on average 900 per day) and BOX4 has the smaller number of observations (less than 50 per year); BOX1 and BOX2 contribute with an average amount of 200 and 115 observations per day, respectively. The criterion used to select the evaluation period to be reported was based on those years with the largest available observations. The spatial distribution of stations that reported more than 80% of the days (above 876 days) was January 2011 to December 2013 (see Figure 1b). Thus, it was selected for evaluation. However, similar results were obtained for 2019 that was a year with the smallest available data round year.

Another important point is that the numbers of stations reported from Brazil (see Figure 1c) have had a sustained decrease, and this trend has not been verified for the number of stations reported from other countries. This alert is important as the referred tendency potentially threatens the capability to accurately represent the atmospheric conditions and to sustain the quality of the products derived with possible implications for both monitoring and modelling efforts.

Even when observed data are representative of the "truth," it is quite common that they are affected by systematic or random errors, even for those collected from automatic stations. Among the main factors causing the errors are (a) ungauged or aged instruments; (b) errors in the acquisition process; (c) errors in the transmission. By virtue of these errors, a quality control, the operational CPTEC/INPE two step quality control, was applied to the dataset studied. In the first step, labelled as objective, any suspicious values are treated in a system that includes outliers remotion (Tukey, 1977), internal check (Baker, 1992) and space–time consistency (Xu *et al*., 2014). After that, in

the second step, labelled as subjective, a meteorologist accepts/rejects data identified in the objective step. All the data depicted in Figure 1a–c has already passed by the quality control.

2.3 | ERA5 reanalysis

The ERA5 is an acronym for the European Centre for Medium-Range Weather Forecasts (ECMWF) fifth generation global reanalysis. The ERA5 two meters temperature (T2m) was combined with observations and are the basis for the computation of the LRT. ERA5 reanalysis succeeds the previous ERA-Interim reanalysis and contains several improvements with respect to its predecessor, which ranges from space–time resolution to improvements in the representation of atmospheric processes. For instance, the horizontal resolution, the number of vertical levels and the enabled time–frequency has changed from (79 km, 60 levels, and 4 times a day or every 6 hr) for the ERA-Interim to (31 km, 137 levels, and 24 times a day or every 1 hr) for the ERA5. The newer reanalysis is now providing a measure of the uncertainty through a 10-members ensemble data-assimilation (EDA) at a coarser resolution of 63 km and a frequency of 8 times a day or every 3 hr. In addition, the representation of different atmospheric conditions has been improved like in the Antarctic Peninsula (Tetzner *et al*., 2019), United States (Hoffmann *et al*., 2019), North America (Tarek *et al*., 2020) and China (Zhang *et al*., 2019). ERA5 combines model data, satellite and observations from all the globe through a data assimilation process (see Hersbach *et al*., 2020). Currently, ERA5 is available since January 1979 to the present with a latency of 5 days through the Copernicus data store (cds.climate.copernicus.eu).

2.4 | Estimate the lapse rate of temperature

To estimate the lapse rate of temperature (LRT), the T2m from the historical 40 years of data (1979–2019) and the GTOPO30 with a resolution of 900 m were used. Observed data were not included for the computation as some regions depicted data shortage. The procedure through which LRT is obtained is as follows: (a) From the hourly ERA5 reanalysis data both Tmax and Tmin were extracted for each day considering the entire studied period. (b) Quarterly means from these fields were computed using daily data from the previous step. (c) For each grid point of the mean fields, an elevation was assigned using the closest elevation data from GTOPO30. (d) To regionalize the computation, the studied domain was divided in four boxes (Figure 1b) taking into account both the elevation and the spatial distribution of moisture over South America since it influences the LRT values (Kattel *et al*., 2013; Li *et al*., 2013). (e) For each selected box a linear fit is performed on temperature and height data to obtain an slope representing the LRT and a linear intercept parameter Co (Equation (1); see also Rolland, 2003; Blandford *et al*., 2008; Minder *et al*., 2010),

$$T = \mathrm{Co} + \mathrm{LRT} * \mathrm{H}, \tag{1}$$

where T represents either Tmax or Tmin in °C is the dependent variable, Co is a linear intercept in °C representing the temperature for the case of H equal to zero, LRT is the lapse rate of temperature ($^{\circ}\mathrm{C}\cdot\mathrm{km}^{-1}$) and H the independent variable (elevation in km). (f) Quarterly means of the LRT values for austral summer (DJF), autumn (MAM), winter (JJA) and spring (SON) were obtained.

2.5 | South American Mapping of Temperature

SAMeT is designed to minimize errors that occur during interpolation of temperature over regions with data scarcity and to contemplate elevation effects due to rugged topography. SAMeT is obtained through the following steps: (a) combine ERA5 with observations, attributing more importance to the observations; (b) adjust temperature data as a function of the LRT. The detailed processes to obtain SAMeT are as depicted in Figure 2.

2.5.1 | Combine ERA5 with observed data

- A bias remotion of the ERA5 using observed data interpolated to the reanalysis grid through ordinary Kriging method.
- Observed data (black dots) are georeferenced with respect to its nearest ERA5 horizontal grid point (shaded; see Figure 2a).
- For grid points in which there exist observations the ERA5 are omitted within a radius of roughly 100 km (see Figure 2b). This is in agreement with the WMO stipulated influence radius for meteorological stations. However, preliminary test using a small period indicates that reducing the influence radius to 50 km improves all the metrics (not shown). Further studies are needed to verify which influence radius represents the observed data.

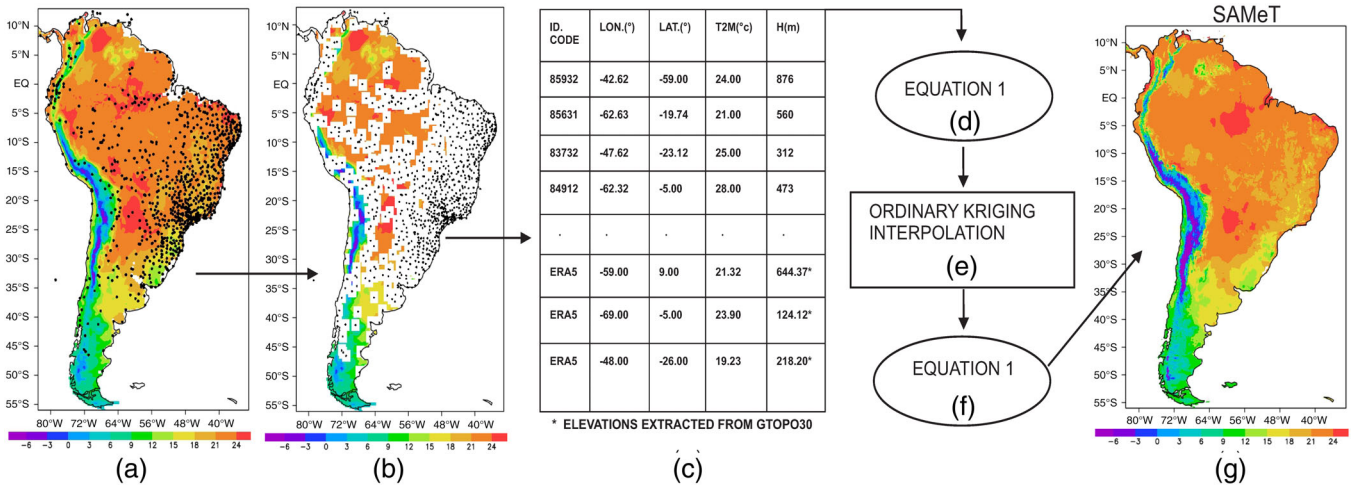

FIGURE 2 Schematic illustration of the processes to obtain SAMeT product; (a) quality controlled observations are georeferenced (black dots) to the ERA5 gridded data (shaded); (b) spatial distribution of the influence radius of the quality controlled observed data into the ERA5 gridded data; (c) tabulation of the data obtained from the observations and ERA5 data; (d–f) Kriging interpolation with adjustment of the LRT; (f) SAMeT product with a 5-km resolution [Colour figure can be viewed at wileyonlinelibrary.com]

- The observations and the unbiased ERA5 data that were not removed are tabulated (see Figure 2c) and used later for the construction of SAMeT.

2.5.2 | Adjustment of the temperature data as a function of LRT

- Temperature data (from the table) are taken to the sea level through a single linear regression (Equation (1)) using LRT values estimated for the box and elevation data for each point (Figure 2d).
- Data taken to the sea level are spatialized to a 5-km resolution using ordinary Kriging interpolation (Figure 2e).
- Finally, the 5-km resolution spatialized data are corrected by the LRT using Equation (1) and an LRT (Figure 2f) for each of the defined boxes, the digital elevation from GTOPO30 to obtain the SAMeT product (Figure 2g).

2.6 | Evaluation methods

This section is devoted to the evaluation of both the LRT estimates and also the performance of SAMeT. The evaluation period was from January 2011 to December 2013. This period was selected due to the larger number of available observations (on average 1,500 observations per day). The adopted scheme is the cross evaluation and consists of a random split of data 90% of the observed data (OBS90) for the generation of the interpolated data and 10% of the observations (OBS10) for evaluation purposes (see also Rozante *et al*., 2020). Figure 3 depicts the cross-validation scheme. The procedure is performed every day throughout the whole evaluated period. From the observational data set (see step 1), an amount of 10% of the data (OBS10) is randomly removed for each of the indicated boxes (see step 2 in the diagram). The remaining data (OBS90) along with GTOPO30, the estimated LRT and the reanalysis ERA5, are used to build SAMeT (step 4). For comparison purposes, OBS90 data are also interpolated using Kriging method, GTOPO30 and a temperature adjustment by using the standard LRT; the product obtained is OBS90i (step 5). The temperature values of the removed points (latitude and longitude) (OBS10) are compared to the closest grid points of ERA5, SAMeT and OBS90i and presented in table (step 6). Information referring to this table is applied to statistical metrics (step 7).

The statistical metrics to evaluate the results were (a) mean error (ME), (b) root-mean-square error (RMSE) and (c) Pearson correlation coefficient (r), as described in the following equations in Table 1.

3 | RESULTS AND DISCUSSIONS

3.1 | Lapse rate of temperature

The results of the linear regressed LRT for both the maximum (LRTmax) and minimum (LRTmin) temperatures estimated for the four boxes used to generate SAMeT are presented in this section. Relative moisture derived from

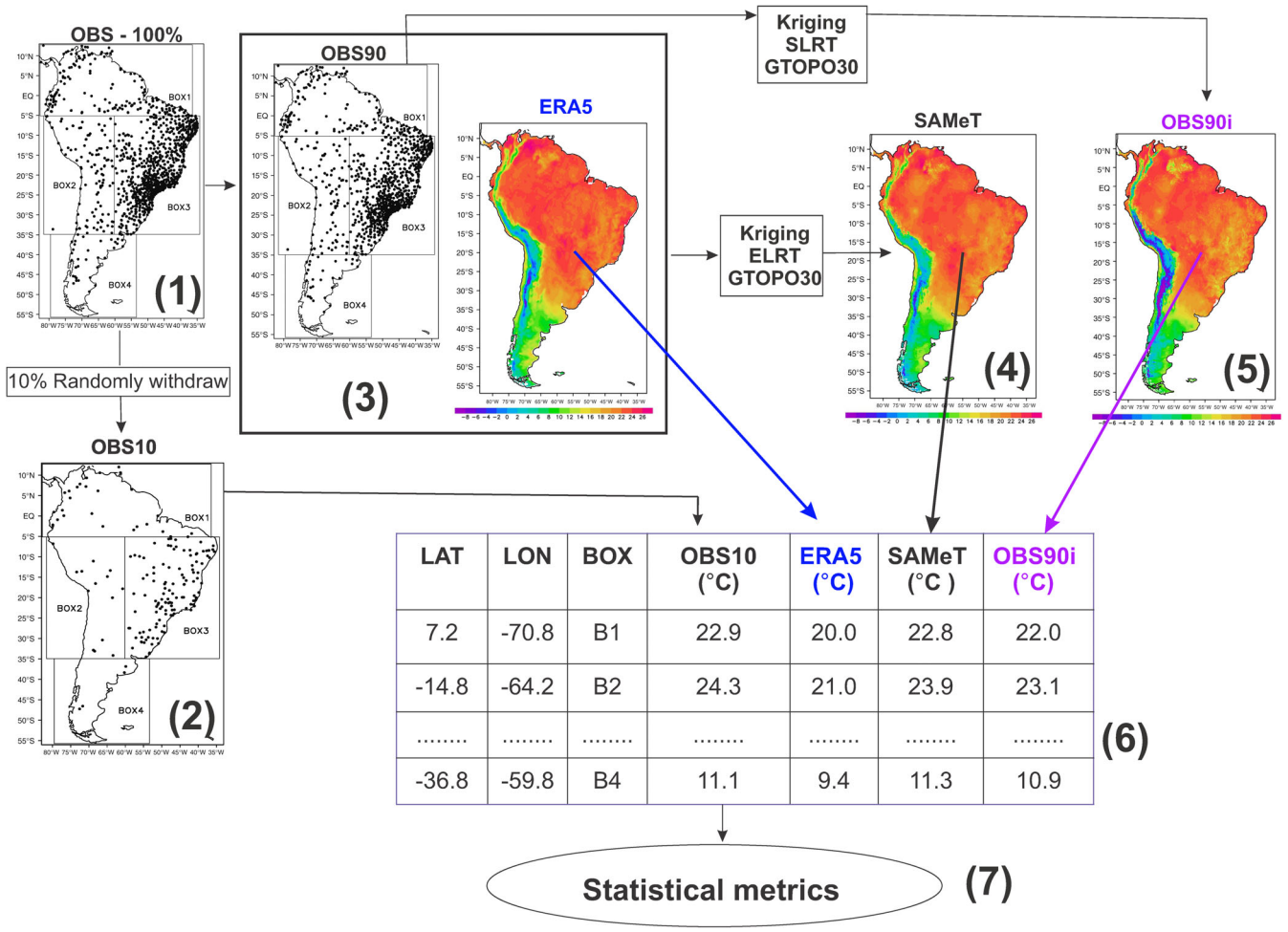

FIGURE 3 Schematic diagram depicting how data was split, to obtain the referential temperature OBS10 to be compared with SAMeT, OBS90i and ERA5 [Colour figure can be viewed at wileyonlinelibrary.com]

TABLE 1 Statistical indices

Statistical index	Equation	Optimum value
Root-mean-square error	$\mathrm{RMSE}=\sqrt{\frac{\sum_{p=1}^{N}(\mathrm{TF}_p-O_p)}{N}}$	0
Mean error	$\mathrm{ME}=\frac{1}{N}\sum_{p=1}^{N}(\mathrm{TF}_p-O_p)$	0
Pearson correlation coefficient	$r=\frac{\sum_{p=1}^{N}(O_p-\overline{O}).(\mathrm{TF}_p-\overline{\mathrm{TF}})}{\sqrt{\left(\left(\sum_{p=1}^{N}(O_p-\overline{O})^2\right)\left(\sum_{p=1}^{N}(\mathrm{TF}_p-\overline{\mathrm{TF}})^2\right)\right)}}$	1

Note: TF is the temperature fields (SAMeT, OBS90i or ERA5); O is the observational data (10% of the available station data are randomly removed); p is the point of station; N is the number of stations.

the ERA5 air temperature and dewpoint were also discussed, since the distinction between dry and wet conditions is of extreme importance in controlling the lapse rate near the surface (Kattel *et al*., 2013). Figure 4 depicts the austral hemisphere seasonal means (summer, DJF; autumn, MAM; winter, JJA and spring, SON) for LRTmax, LRTmin and relative moisture for the four studied boxes. BOX1 which is located into the equatorial band (see Figure 4a) either the LRT as well as the relative moisture remains almost constant along the different seasons, with mean values of $-3.82°\mathrm{C}\cdot\mathrm{km}^{-1}$ and 83%, respectively. BOX2 corresponds to the Andean region

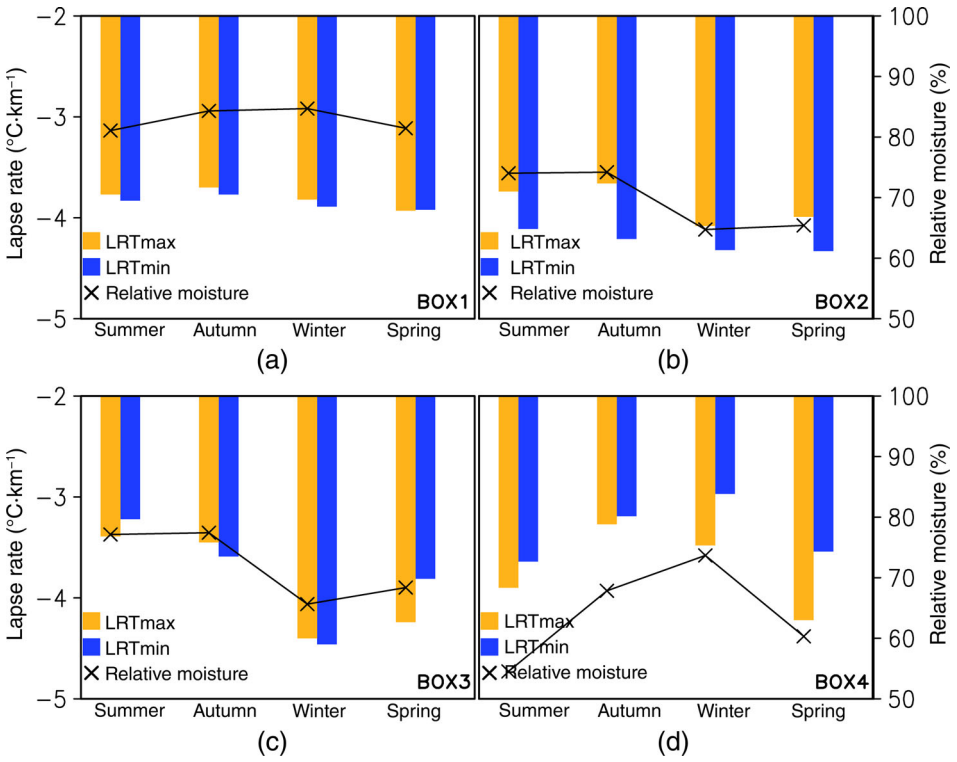

FIGURE 4 Quarterly means of LRTmax, LRTmin and relative moisture for BOX1 (a), BOX2 (b), BOX3 (c) and BOX4 (d), respectively [Colour figure can be viewed at wileyonlinelibrary.com]

(Figure 4b) consequently records the largest surface elevations. BOX2 depicts a pronounced variation of the LRTmax along the different seasons. For summer and autumn the mean LRTmax was $-3.70°C·km^{-1}$ and LRTmin was $-4.16°C·km^{-1}$, while for winter and spring mean LRTmax $-4.03°C·km^{-1}$ and LRTmin $-4.32°C·km^{-1}$. It is noticeable that the slight increase of the LRT for the winter and spring coincide with a light increase in the moisture (about 10%). In BOX2 LRTmin is larger than LRTmax for all the seasons. In a recent study, Navarro-Serrano *et al.* (2020) using observed data for the Andean region of Equator and Peru, which corresponds to BOX1 and BOX2, obtained similar values for the LRT than those obtained here; thus, ERA5 can be used to estimate LRT in regions with lack of observed data. BOX3 (Figure 4c), which is located mostly over Brazil, depicts a pattern with moisture of around 77% for summer and autumn, and 67% for winter and spring. Mean values of LRT for summer and autumn are LRTmax $-3.42°C·km^{-1}$ and LRTmin $-3.40°C·km^{-1}$. For winter LRT is $-4.40°C·km^{-1}$ for LRTmax and $-4.46°C·km^{-1}$ for LRTmin. For spring the LRT was smaller (with respect to winter) with LRTmax $-4.24°C·km^{-1}$ and LRTmin $-3.81°C·km^{-1}$. BOX4 (Figure 4c), which is located to the south of the continent, depicts a pronounced seasonal pattern for the moisture, with values of around 55% during summer and 74% during winter. This characteristic is reflected on the seasonal pattern for LRT with maximum values during summer and spring and minimum values during autumn and winter. Generally, temperature lapse rates are weaker under moister than under drier conditions (Blandford *et al.*, 2008; Minder *et al.*, 2010), which could be associated to the larger thermal inertia of the water vapour, the propention to saturation with the decrease of temperature and also to the latent heat released from condensation. All LRT computed in the present study based on ERA5 data are lower than those obtained from standard atmospheres ($-6.5°C·km^{-1}$). This indicates that the temperature would be warmer than those estimated on the basis of standard LRT. Several studies have described the space and time variability of the LRT, and consistently reported values for LRT smaller than $-6.50°C·km^{-1}$ over different regions like: the Appalachian mountains (Bolstad *et al.*, 1998), Canadian rocky mountains (Shea *et al.*, 2004), Northern Canadian islands (Marshall *et al.*, 2007), and Arctic glaciers (Gardner *et al.*, 2009).

In order to verify whether the temperature field based on the estimated LRT (ELRT) produces consistent spatial, it was compared to a similar field that was spatialized using a standard atmosphere LRT (SLRT = $-6.5°C·km^{-1}$). Interpolations using OBS90 SLRT and ELRT for the years 2011–2013. Cross-validation was used against OBS10 and although daily data are generated, results were presented through quarterly means.

The averaged RMSE for each of the studied boxes is depicted in Figure 5. The errors for temperature obtained using ELRT are smaller than those obtained through

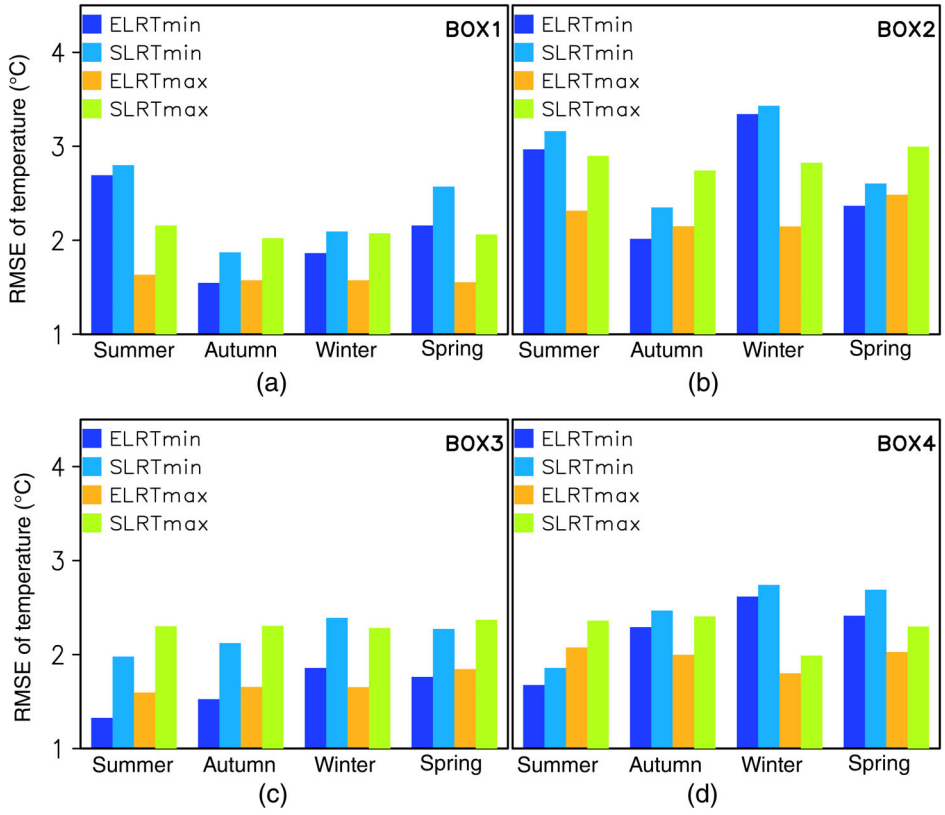

FIGURE 5 Quarterly mean of the RMSE for the maximum temperatures and minimum temperatures spatialized using SLRT and ELRT for BOX1 (a), BOX2 (b), BOX3 (c) and BOX4 (d) [Colour figure can be viewed at wileyonlinelibrary.com]

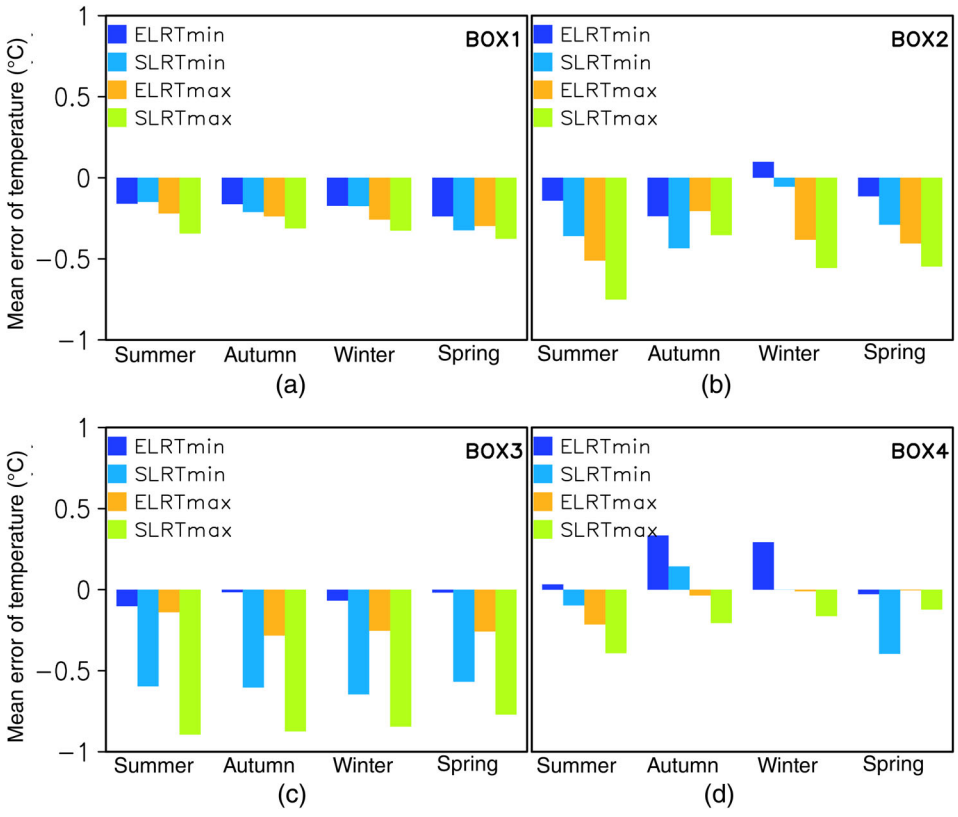

FIGURE 6 Quarterly mean error of the maximum temperatures and minimum temperatures spatialized using SLRT and ELRT for BOX1 (a), BOX2 (b), BOX3 (c) and BOX4 (d) [Colour figure can be viewed at wileyonlinelibrary.com]

SLRT. For all the analysed boxes, the seasonal variability of the errors is pronounced for the minimum temperature, while they are almost constant for the maximum temperature. The largest errors for BOX1 (Figure 5a) are obtained during summer (2.75°C). The RMSE for Tmax remains almost constant along the seasons being 2.71°C (SLRT) and 1.50°C (ELRT). In BOX2 (Figure 5b), which corresponds to the Andean region (largest elevations), is also the area with the largest errors. The best performances of the product using ELRT are obtained in BOX3 (Figure 5c). While BOX4 is less sensitive to the use of ELRT (Figure 5d). The analysis of the mean error (Figure 6) shows a clear tendency to underestimate the temperature values (SLRT). The use of the ELRT contributes to reducing the negative bias, mainly for BOX3 (Figure 6c). Further studies can be conducted in order to achieve a better characterization of the region to which the LRT spatialization must be applied. The use of SLRT tends to produce negative bias and in part this explains the tendency to underestimate.

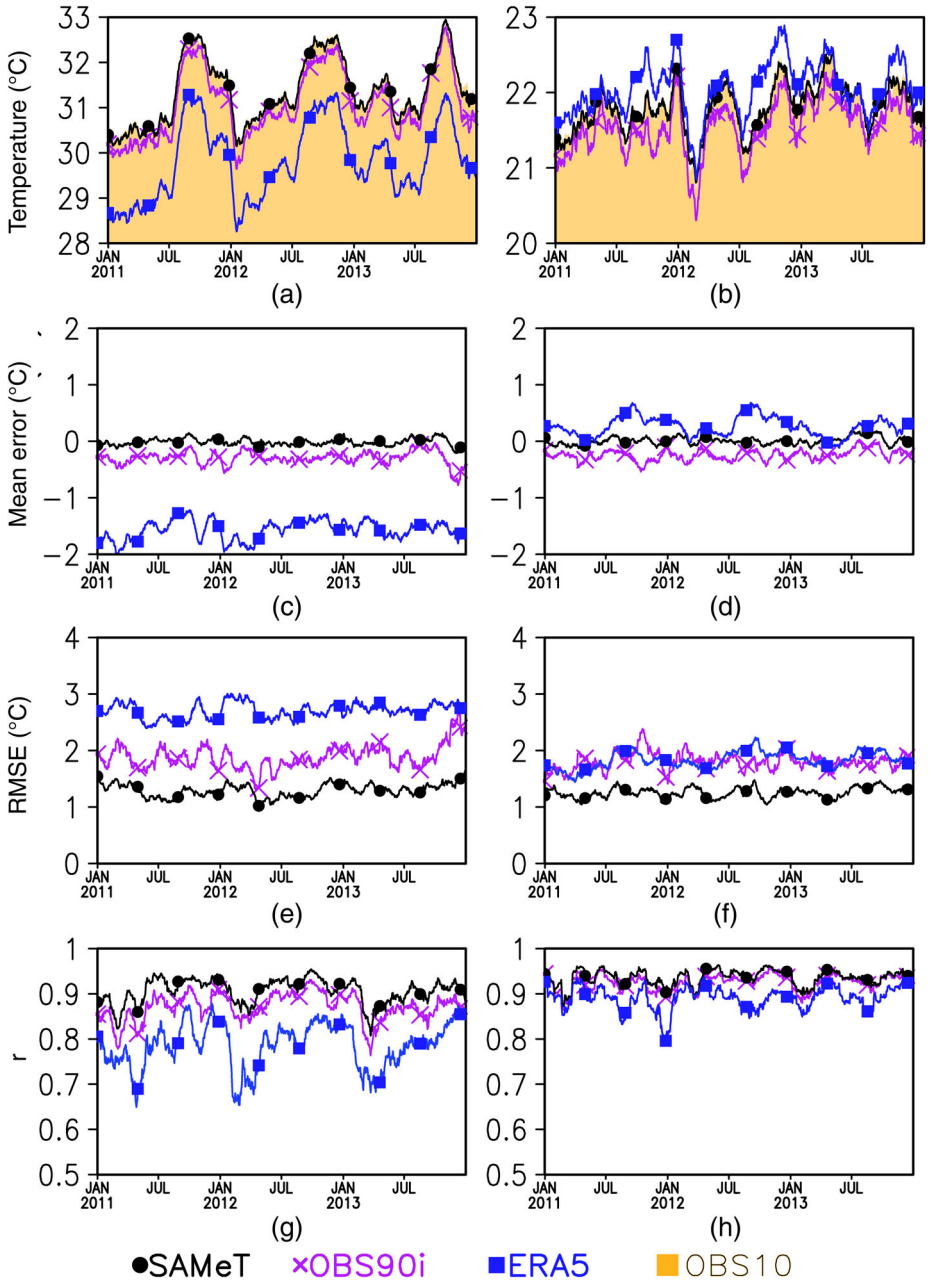

FIGURE 7 BOX1 time series for temperature (a, b); mean error (c, d); RMSE (e, f); Pearson correlation coefficient (g, h) for SAMeT (closed-circle-line), OBS90i (X-line), ERA5 (closed-squared line). Left panel is for Tmax while right panel is for Tmin. Shaded in grey if for OBS10 data [Colour figure can be viewed at wileyonlinelibrary.com]

3.2 | South American Mapping of Temperature

In this section an assessment of SAMeT for 2011–2013 is depicted for all the studied boxes. For the sake of comparison, the ERA5 and OBS90i will also be discussed. The results and the statistical indexes for the maximum (Tmax) and minimum (Tmin) temperature were depicted for each of the studied boxes. For each day of the time evolution, an average for temperature and statistical indices (obtained from OBS10) is computed. A 7-day running mean was also applied to both temperature and statistical indices.

The general characteristics are well represented considering the different data sources used (i.e., SAMeT, ERA5 and OBS90i) for the whole selected period and every selected box, including a representation of the annual cycle by all three data sources. However, SAMeT performs better in terms of BIAS and RMSEs and also depicts higher Pearson correlations when compared to ERA5 and OBS90i. ERA5 tends to depict a shorter diurnal range, with negative bias (underestimation) for Tmax and positive bias (overestimation) for Tmin. OBS90i has a negative bias (underestimation) for both Tmax and Tmin; this could be related to the largest lapse rate used to obtain OBS90i.

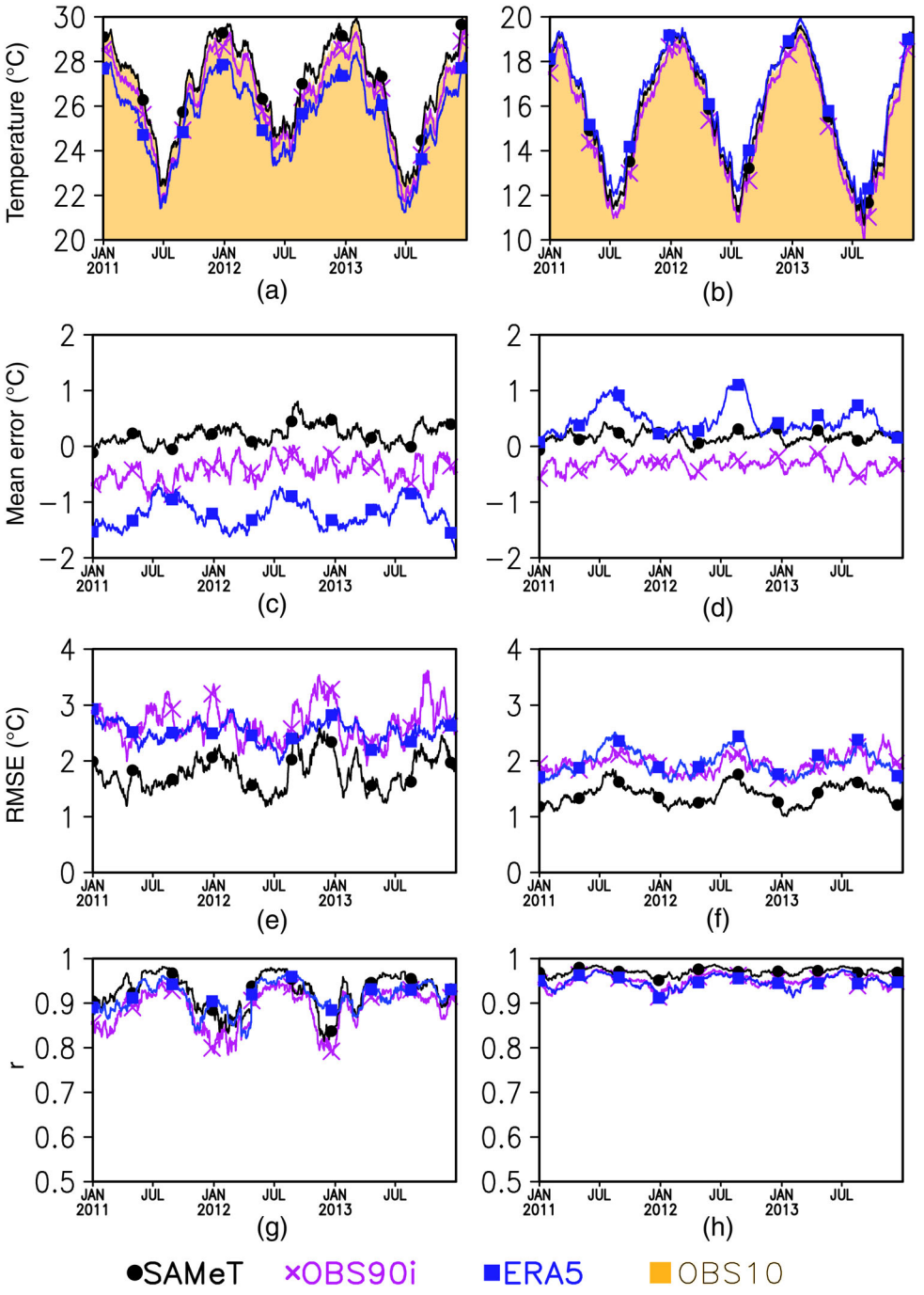

FIGURE 8 BOX2 time series for temperature (a, b); mean error (c, d); RMSE (e, f); Pearson correlation coefficient (g, h) for SAMeT (closed-circle-line), OBS90i (X-line), ERA5 (closed-squared line). Left panel is for Tmax while right panel is for Tmin. Shaded in grey if for OBS10 data [Colour figure can be viewed at wileyonlinelibrary.com]

BOX1, located over the equatorial area, depicts the smaller variations in temperature along their annual cycle, being smaller than 2°C for Tmax (Figure 7a) and 1°C for Tmin (Figure 7b). For both Tmax and Tmin SAMeT's data are closer to the observed data and depict a mean error quite close to zero. Also, OBS90i and ERA5 tend to underestimate Tmax with ERA5 depicting the largest mean error; ERA5 overestimates Tmin (Figure 7c, d). SAMeT also displayed the smaller values of RMSE for both Tmax and Tmin, with ERA5 performed worse than the other for Tmax and almost the same as OBS90i for Tmin (Figure 7e,f). Pearson correlation is also favouring SAMeT, performing better than the second better correlated OBS90i and the third is ERA5. Furthermore, improvements with SAMeT are larger for Tmax (Figure 7g,h).

For BOX2, that includes an Andean region sector with the highest mountains as well as part of the Amazon vessel. For this BOX, a larger range of temperatures between summer and winter are noted with SAMeT depicting values closer to the observations (Figure 8a,b); the mean diurnal range difference (Tmax – Tmin) can be

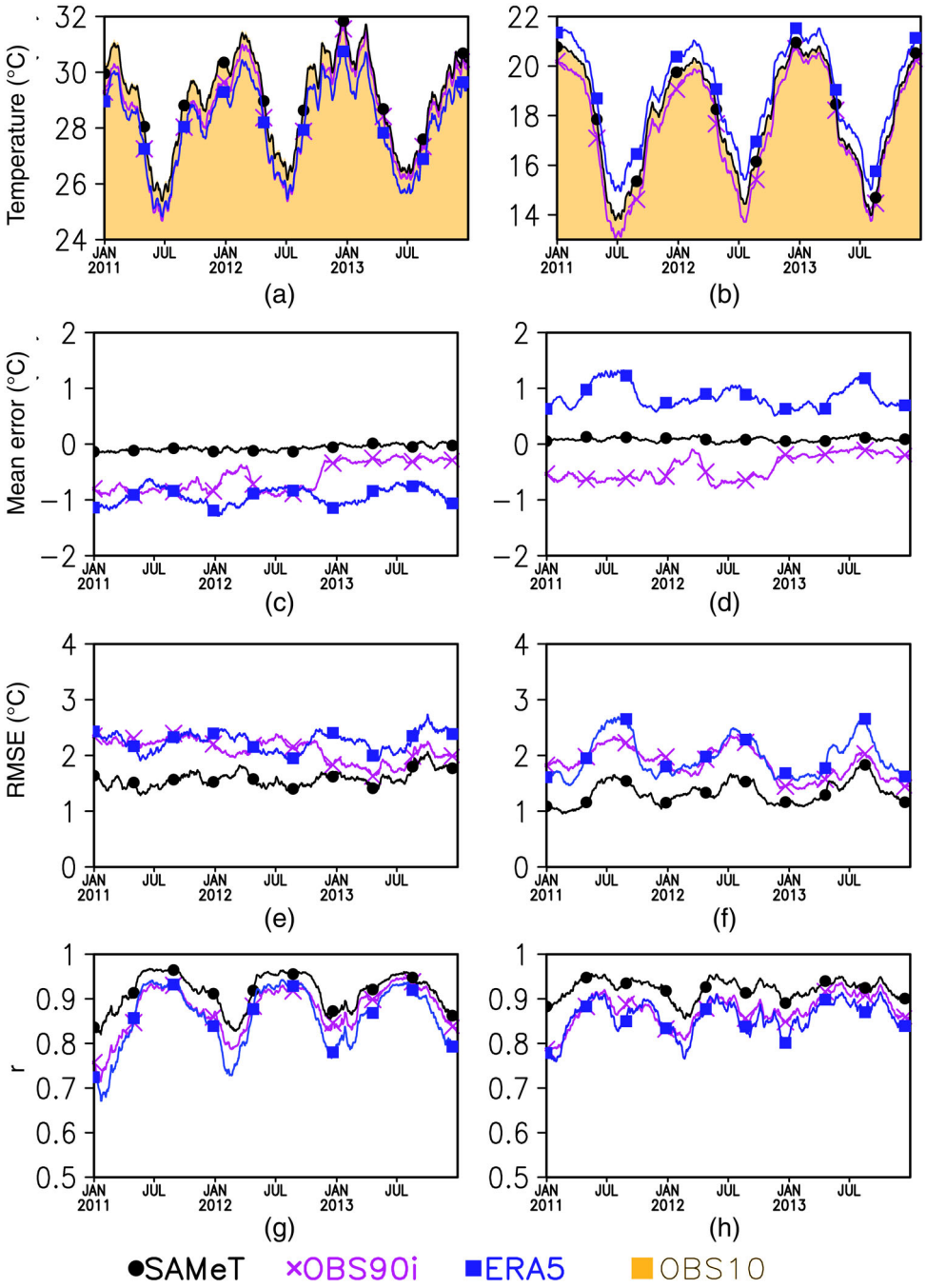

FIGURE 9 BOX3 time series for temperature (a, b); mean error (c, d); RMSE (e, f); Pearson correlation coefficient (g, h) for SAMeT (closed-circle-line), OBS90i (X-line), ERA5 (closed-squared line). Left panel is for Tmax while right panel is for Tmin. Shaded in grey if for OBS10 data [Colour figure can be viewed at wileyonlinelibrary.com]

as large as 11°C (not shown). ERA5 and OBS90i underestimate Tmax, with ERA5 displaying the larger bias. SAMeT has the smallest mean error for Tmax and Tmin, tending to overestimate (Figure 8c,d). The mean error for the period was about 0.2°C. For winter, ERA5 depicts a contrasting behaviour with smaller errors for Tmax and larger errors for Tmin. SAMeT performs better than the other data sources for both Tmax and Tmin, and although Tmin depicts smaller RMSEs, the improvements against other data sources are larger for Tmax (Figure 8e,f). For Tmin, the largest RMSEs are obtained during winter (Figure 8f). For ERA5 and OBS90i there is an intra-annual alternancy of the RMSE skill. SAMeT also displays the best Pearson correlation coefficient Figure 8g,h); the correlations are quite close for the data sources used and there is a notorious decrease of the correlation for warmer seasons. The variability in correlations is more accentuated for Tmax and more flat for Tmin, probably associated with other related variables not considered.

BOX3 is the region with the larger number of observations. It could be seen that SAMeT is closest to the

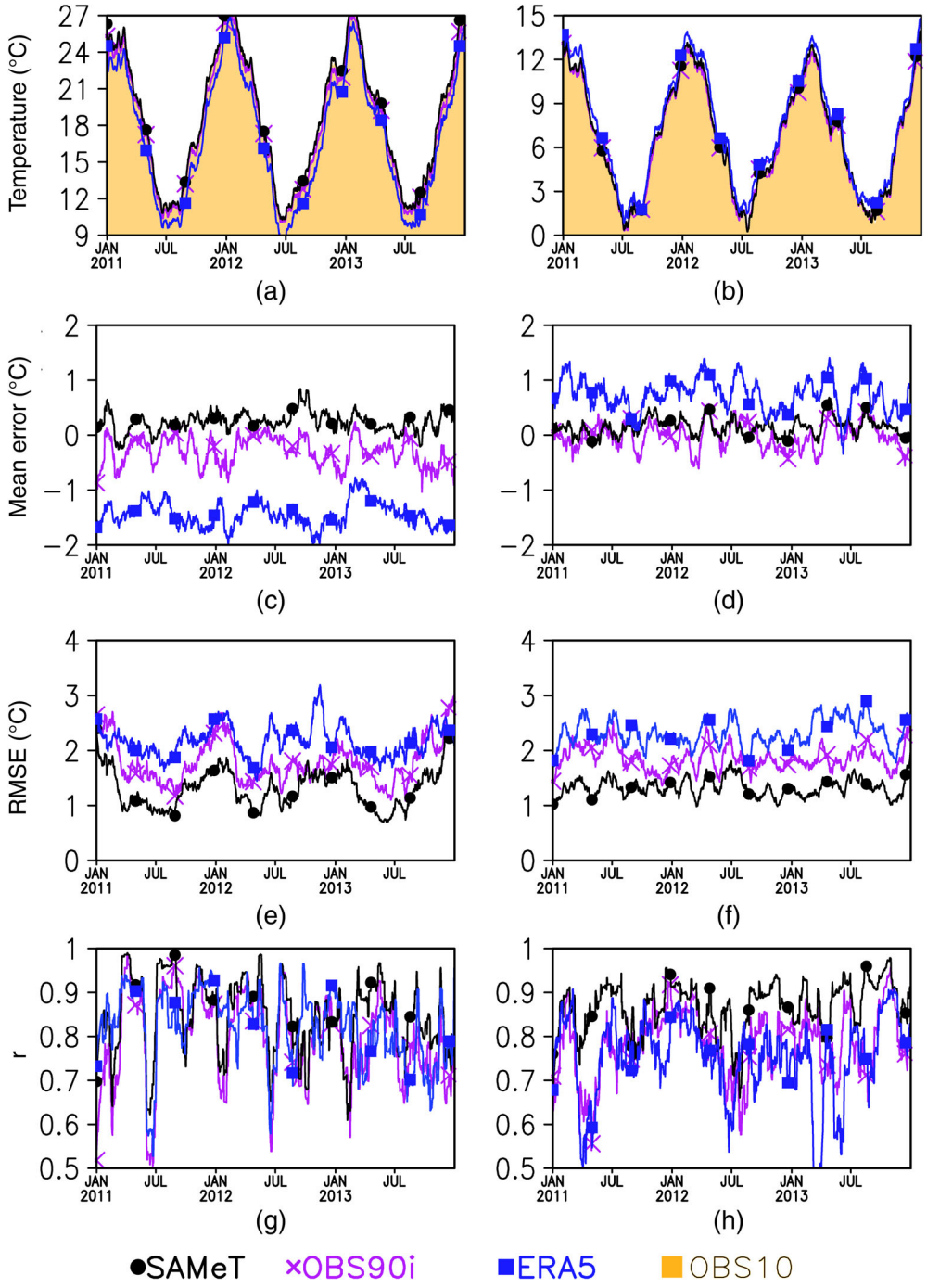

FIGURE 10 BOX4 time series for temperature (a, b); mean error (c, d); RMSE (e, f); Pearson correlation coefficient (g, h) for SAMeT (closed-circle-line), OBS90i (X-line), ERA5 (closed-squared line). Left panel is for Tmax while right panel is for Tmin. Shaded in grey if for OBS10 data [Colour figure can be viewed at wileyonlinelibrary.com]

observations (Figure 9a,b). For Tmax, ERA5 and OBS90i tend to underestimate. For Tmin, ERA5 tends to overestimate, while OBS90i underestimate (Figure 9b); the differences are relatively large, peaking 1.5°C during austral winter. SAMeT also depicts the smaller mean error for both Tmax and Tmin with ERA5 displaying the largest mean errors (Figure 9c,d). ERA5 tends to display a flattest diurnal cycle (smaller Tmax and larger Tmin) than the other data sources. Regarding the RMSE, SAMeT also depicts the smaller errors (Figure 9e,f) being of about 1.5 and 1.3°C for Tmax and Tmin, respectively. Tmin presents a more pronounced annual variability with largest errors during winter (Figure 9f). ERA5 and OBS90i present a pronounced annual variability smaller error (1.6°C) for austral summer and larger values for austral winter (2.7°C) (Figure 9f). In addition, the Pearson correlation coefficient also indicates that SAMeT performs better than the other data sets (Figure 9g,f). OBS90i and ERA5 depict similar correlations, OBS90i depicts slightly larger correlations than ERA5 (Figure 9g).

For BOX4, the region with the lowest number of observations, SAMeT and OBS90i are similar for the whole period. ERA5 displays smaller temperatures for Tmax and larger for Tmin (Figure 10a,b). Although SAMeT and OBS90i are close, it must be noted that SAMeT overestimate (on average 0.2°C), whereas OBS90i underestimate (on average −0.3°C). ERA5 underestimates (on average −1.5°C) for Tmax and overestimates (on average 0.7°C) for Tmin for the whole period (Figure 10c,d). SAMeT also depicts the smaller values of RMSE for Tmax and Tmin (on average 1.3°C) (Figure 10e,f), whereas the ERA5 depicts the larger RMEs. The correlation displays a substantial variation along the period (Figure 10g,h). The correlation for Tmin shows that SAMeT performs better than the other products, while for Tmax the correlation oscillates along the period. Averages indicate that correlations for Tmax are slightly better for SAMeT (0.85) than for OBS90i (0.80) and ERA5 (0.82) (not shown).

As an example, the spatialized Tmax and Tmin using SAMeT, OBS90i and ERA5 are depicted for January 10,

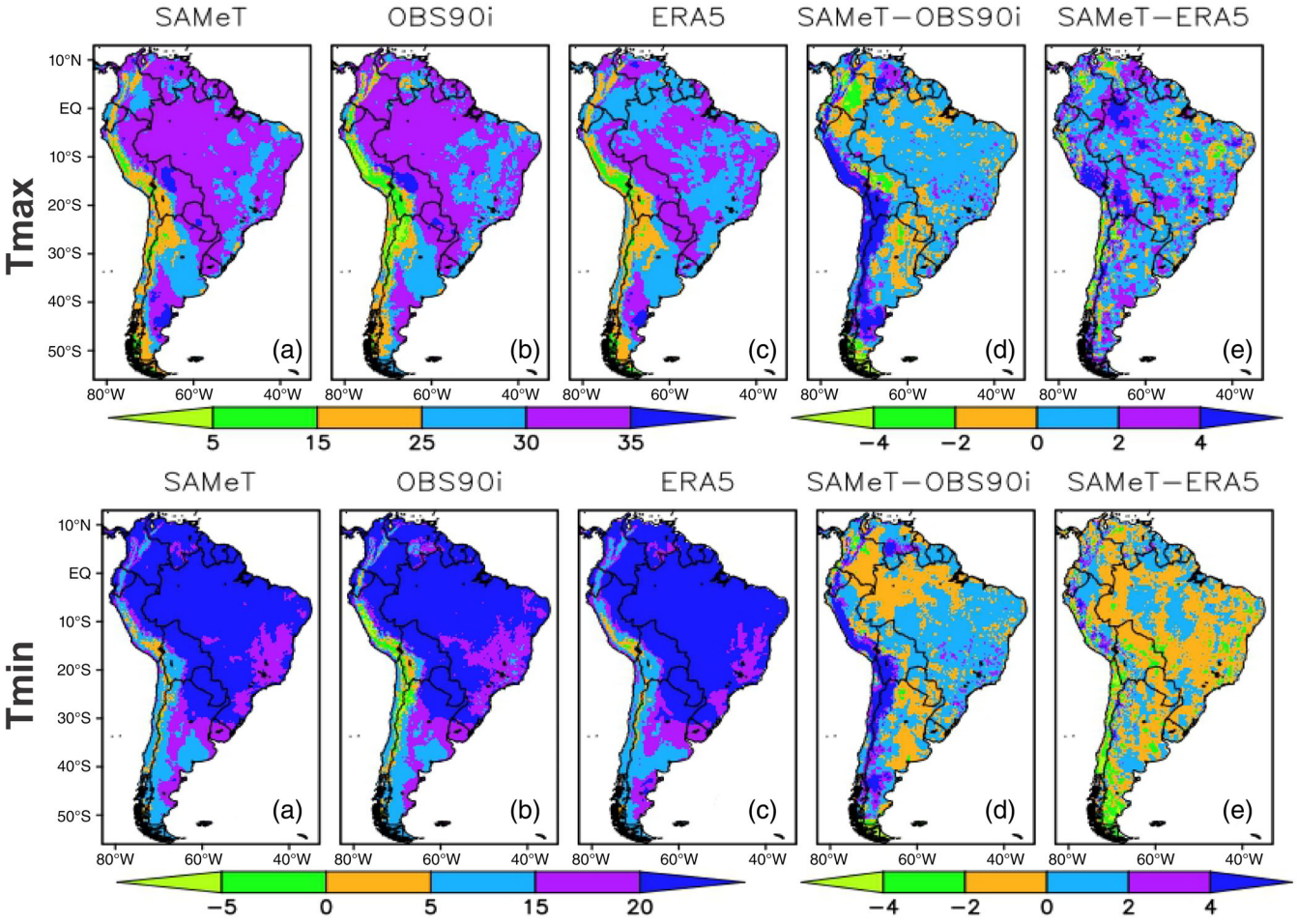

FIGURE 11 Spatial distribution of SAMeT (a, f), OBS90i (b, g) and ERA5 (c, h) for Tmax and Tmin, along with the differences between SAMeT and OBS90i (d, i), and SAMeT and ERA 5 (e, j) for January 10, 2011 [Colour figure can be viewed at wileyonlinelibrary.com]

2011. The differences between SAMeT, OBS90i and the ERA5 interpolated to the SAMeT grid are also presented (Figure 11). The spatial fields obtained for SAMeT are similar to those obtained through the other data sources, although some differences can be noted, like for example SAMeT is smoother than ERA5 (Figure 11a–c,f–h). However, the largest differences are found between SAMeT and OBS90i along the Andean region (Figure 11d,i). Those differences are partially caused by the use of SLRT in OBS90i, which is stronger than ELRT used in SAMeT and responsible for smaller temperatures obtained for OBS90i. The narrower diurnal range of ERA5 when compared against SAMeT is also evidenced, with a warmer Tmax (Figure 11e) and a cooler Tmin for SAMeT (Figure 11j).

4 | CONCLUSIONS AND PERSPECTIVE

A new methodology for spatialization of temperature fields that corrects elevational aspects coined as the South American Mapping of Temperature (SAMeT) was developed. SAMeT makes use of independently estimated LRT (ELRT) for Tmax and Tmin, a combination of observed data, ERA5 reanalysis and GTOPO30. The ELRT was computed via simple linear regression using 40 years of unbiased ERA5 reanalysis data and made valid for different seasons and for four subdomains selected over South America. The spatialization gave rise to a twice a day spatial field of temperature also named SAMeT. Cross validation of SAMeT's temperature fields against observed data (OBS10) not used in the constructions of SAMeT are performed. The evaluation was performed for the 2011–2013 period, which is one of the periods with more available observational data. However, evaluations were also performed for 2019 which was a period with few reported observational data. Results were contrasted to similar validations using an alternative spatialized field (OBS90i) that use the standard LRT (SLRT) and also against ERA5 reanalysis data.

The ELRT is weaker than the moist SLRT ($-6.5°C \cdot km^{-1}$) and likewise is weaker under moist conditions than over dry conditions. This is related to the larger thermal inertia of the humid air, yet the release of latent heat at higher elevations has also been suggested (Blandford *et al*., 2008; Minder *et al*., 2010). The weaker ELRT suggests a distinction between superficial lapse rate and free atmosphere lapse rate (Gardner *et al*., 2009; Wang *et al*., 2018; Lute and Abatzoglou, 2021). As a consequence, there is a tendency to underestimate temperature fields corrected by the elevation when the SLRT is used. The spatialization of temperature obtained through an ELRT in SAMeT improved the metrics when compared to the other spatialization (OBS90i) that uses SLRT and also compared to the ERA5 reanalysis. The comparisons were based on maximum and minimum temperatures, within the four different regions represented by defined boxes. ERA5 tends to underestimate Tmax and overestimate Tmin, consequently the range of extremes related to ERA5 are narrower. Systematic errors for ERA5 were also reported in other studies (e.g., Bandhauer *et al*. (2020) for Scandinavia, Carpatos and Alpes or Johannsen *et al*. (2019) for the Iberian Peninsula).

In general terms, the spatialization of temperature improves data obtained exclusively from ERA5 reanalysis. In particular SAMeT improves results obtained through spatialization with the standard lapse rate (OBS90i), for instance OBS90i underestimates temperature within all the boxes (negative bias). The ELRT produces smaller rates for the decrease of temperature with height. This is not a peculiar behaviour for South America as it has been already identified for the Himalayas (Romshoo *et al*., 2018), the Tibetan Plateau (Wang *et al*., 2018; Zhang *et al*., 2019), China (Qin *et al*., 2018) and for the Arctic (Gardner *et al*., 2009). The annual cycle is also well represented by all data sources used; however, SAMeT displayed values closest to the observations. SAMeT also depicts smaller RMSEs and higher values for Pearson correlations.

We also would like to stress that our selected approach was based on practical results. In fact, when we used the zeroth order approach (i.e., using a unique LRT for the whole South American continent, based on an EOF analysis of the temperature), we already produced a surface temperature product that resulted in a better surrogate for OBS90i and ERA5 reanalysis. The metrics used for this assertion were exactly the same as those reported in the present report. Moreover, when we performed the separation in boxes, we obtained even better results than those using a unique LRT for the whole SA. Thus, based on the obtained results, we decided to report the submitted work. In order to be useful for a diversity of users and researchers, daily values of SAMeT has been made operationally available on the website of the National Institute for Space Research (INPE) (http://ftp.cptec.inpe.br/modelos/tempo/SAMeT).

Finally, we would like to say that there are a number of lines in course for future improvements (some of those were suggested by the anonymous reviewers). The use of MODIS land surface temperature and emissivity data can be used as another source for kilometre-scale high resolution temperature datasets. Furthermore, we also recognize that there are technically superior and potentially better approaches for data regionalization than the

reported here. A future development for SAMeT includes the use of clusterization before the ELRT is computed. Spatial clustering aims to identify contrasting regimes that merit a separate lapse rate (Lute and Abatzoglou, 2021) and also to distinguish regimes that can be grouped together. There exist options for clusterization like *k*-means, which englobes techniques used to group statistically and objectively data that shares common characteristics allowing to develop products targeting specific groups. At the heart of data clustering are the measures for dissimilarities, the basic measurement are the Euclidean distance, but other metrics like Manhattan dissimilarity, correlations, cross-entropy and topoclimatic dissimilarity approach (TDA) are also used (Lute and Abatzoglou, 2021). Special considerations must be taken for the clusterization of time series, because correlations with a lag, might erroneously classify a group of stations as further apart. Recent interactions with users of SAMeT also suggest that the development of a companion product for the dew point temperature could be beneficial for atmospheric, hydrological, agriculture and ecology modelling, as well as for the design of a diverse gama of new products useful for monitoring purposes. We have also performed preliminary research and noted that a reduction of the influence radius around stations over mountainous regions results in further improvements of the metrics. We expect to report the ongoing work in a subsequent research paper.

ORCID

José Roberto Rozante https://orcid.org/0000-0002-1105-6988
Enver Ramirez https://orcid.org/0000-0002-4678-6382
Alex de Almeida Fernandes https://orcid.org/0000-0003-1520-5896

REFERENCES

Alvarez-Varas, R., Berzins, R., Bilo, K., Chevalier, J., Chevallier, D., de Thoisy, B., Fallabrino, A., Cruz, M.G., Kelez, S., Lopez-Mendilaharsu, M., Marcovaldi, M.A., Mast, R.B., Medrano, C., Miranda, C., Nalovic, M.A., Prosdocimi, L., Rguez-Barón, J.M., Santos, A., Soares, L., Thome, J., Vallejo, F. and Vélez-Rubio, G. (2016) *Sea Turtles of South America*, Vol. 11. Kentfield, CA: The State of the World's Sea Turtles, pp. 16–27.

Arnold, N.S., Rees, W.G., Hodson, A.J. and Kohler, J. (2006) Topographic controls on the surface energy balance of a high Arctic valley glacier. *Journal of Geophysical Research: Earth Surface*, 111(F2), F02011. https://doi.org/10.1029/2005JF000426.

Baker, N.L. (1992) Quality control for the navy operational atmospheric database. *Weather and Forecasting*, 7(2), 250–261. https://doi.org/10.1175/1520-0434(1992)007<0250:QCFTNO>2.0.CO;2.

Bandhauer, M., Isotta, F., Frei, C., Lussana, C., Tveito, O.E., Lakatos, M. and Bahari, Z. (2020) *Summary report of the coordinated comparison between pan-European and regional datasets in support of the user guidance*. Reading, United Kingdom: Copernicus, p. 186.

Blandford, T.R., Humes, K.S., Harshburger, B.J., Moore, B.C., Walden, V.P. and Ye, H. (2008) Seasonal and synoptic variations in near-surface air temperature lapse rates in a Mountainous Basin. *Journal of Applied Meteorology and Climatology*, 47 (1), 249–261. https://doi.org/10.1175/2007JAMC1565.1.

Bolstad, P.V., Swift, L., Collins, F. and Régnière, J. (1998) Measured and predicted air temperatures at basin to regional scales in the southern Appalachian mountains. *Agricultural and Forest Meteorology*, 91(3), 161–176. https://doi.org/10.1016/S0168-1923(98)00076-8.

Chappell, A., Renzullo, L.J., Raupach, T.H. and Haylock, M. (2013) Evaluating geostatistical methods of blending satellite and gauge data to estimate near real-time daily rainfall for Australia. *Journal of Hydrology*, 493, 105–114. https://doi.org/10.1016/j.jhydrol.2013.04.024.

Chen, F., Yang, X., Ji, C., Li, Y., Deng, F. and Dong, M. (2019) Establishment and assessment of hourly high-resolution gridded air temperature data sets in Zhejiang, China. *Meteorological Applications*, 26(3), 396–408. https://doi.org/10.1002/met.1770.

Córdova, M., Célleri, R., Shellito, C.J., Orellana-Alvear, J., Abril, A. and Carrillo-Rojas, G. (2016) Near-surface air temperature lapse rate over complex terrain in the southern Ecuadorian Andes: implications for temperature mapping. *Arctic, Antarctic, and Alpine Research*, 48(4), 673–684. https://doi.org/10.1657/AAAR0015-077.

Dinku, T., Hailemariam, K., Maidment, R., Tarnavsky, E. and Connor, S. (2014) Combined use of satellite estimates and rain gauge observations to generate high-quality historical rainfall time series over Ethiopia. *International Journal of Climatology*, 34(7), 2489–2504. https://doi.org/10.1002/joc.3855.

Dodson, R. and Marks, D. (1997) Daily air temperature interpolated at high spatial resolution over a large mountainous region. *Climate Research*, 8, 1–20. https://doi.org/10.3354/cr008001.

Essou, G.R.C., Brissette, F. and Lucas-Picher, P. (2017) Impacts of combining reanalyses and weather station data on the accuracy of discharge modelling. *Journal of Hydrology*, 545, 120–131. https://doi.org/10.1016/j.jhydrol.2016.12.021.

Fuentes, M. and Raftery, A.E. (2005) Model evaluation and spatial interpolation by Bayesian combination of observations with outputs from numerical models. *Biometrics*, 61(1), 36–45. https://doi.org/10.1111/j.0006-341X.2005.030821.x.

Gardner, A.S., Sharp, M.J., Koerner, R.M., Labine, C., Boon, S., Marshall, S.J., Burgess, D.O. and Lewis, D. (2009) Near-surface temperature lapse rates over Arctic glaciers and their implications for temperature downscaling. *Journal of Climate*, 22(16), 4281–4298. https://doi.org/10.1175/2009JCLI2845.1.

Garreaud, R.D., Vuille, M., Compagnucci, R. and Marengo, J. (2009) Present-day South American climate. *Palaeogeography, Palaeoclimatology, Palaeoecology*, 281(3), 180–195. https://doi.org/10.1016/j.palaeo.2007.10.032.

Grimes, D.I.F., Pardo-Igúzquiza, E. and Bonifacio, R. (1999) Optimal areal rainfall estimation using raingauges and satellite data. *Journal of Hydrology*, 222(1), 93–108. https://doi.org/10.1016/S0022-1694(99)00092-X.

Hamlet, A.F. and Lettenmaier, D.P. (2005) Production of temporally consistent gridded precipitation and temperature fields for the

continental United States. *Journal of Hydrometeorology*, 6(3), 330–336. https://doi.org/10.1175/JHM420.1.

Harlow, R.C., Burke, E.J., Scott, R.L., Shuttleworth, W.J., Brown, C. M. and Petti, J.R. (2004) Derivation of temperature lapse rates in semi-arid South-Eastern Arizona. *Hydrology and Earth System Sciences*, 8(6), 1179–1185.

Hersbach, H., Bell, B., Berrisford, P., Hirahara, S., Horányi, A., Muñoz-Sabater, J., Nicolas, J., Peubey, C., Radu, R., Schepers, D., Simmons, A., Soci, C., Abdalla, S., Abellan, X., Balsamo, G., Bechtold, P., Biavati, G., Bidlot, J., Bonavita, M., Chiara, G.D., Dahlgren, P., Dee, D., Diamantakis, M., Dragani, R., Flemming, J., Forbes, R., Fuentes, M., Geer, A., Haimberger, L., Healy, S., Hogan, R.J., Hólm, E., Janisková, M., Keeley, S., Laloyaux, P., Lopez, P., Lupu, C., Radnoti, G., de Rosnay, P., Rozum, I., Vamborg, F., Villaume, S. and Thépaut, J.-N. (2020) The ERA5 global reanalysis. *Quarterly Journal of the Royal Meteorological Society*, 146(730), 1999–2049. https://doi.org/10.1002/qj.3803.

Hoffmann, L., Günther, G., Li, D., Stein, O., Wu, X., Griessbach, S., Heng, Y., Konopka, P., Müller, R., Vogel, B. and Wright, J.S. (2019) From ERA-Interim to ERA5: the considerable impact of ECMWF's next-generation reanalysis on Lagrangian transport simulations. *Atmospheric Chemistry and Physics*, 19(5), 3097–3124. https://doi.org/10.5194/acp-19-3097-2019.

Insel, N., Poulsen, C.J. and Ehlers, T.A. (2010) Influence of the Andes Mountains on South American moisture transport, convection, and precipitation. *Climate Dynamics*, 35(7), 1477–1492. https://doi.org/10.1007/s00382-009-0637-1.

Jaglom, W.S., McFarland, J.R., Colley, M.F., Mack, C.B., Venkatesh, B., Miller, R.L., Haydel, J., Schultz, P.A., Perkins, B., Casola, J.H., Martinich, J.A., Cross, P., Kolian, M.J. and Kayin, S. (2014) Assessment of projected temperature impacts from climate change on the U.S. electric power sector using the Integrated Planning Model®. *Energy Policy*, 73, 524–539. https://doi.org/10.1016/j.enpol.2014.04.032.

Jia, B., Xie, Z., Dai, A., Shi, C. and Chen, F. (2013) Evaluation of satellite and reanalysis products of downward surface solar radiation over East Asia: spatial and seasonal variations. *Journal of Geophysical Research: Atmospheres*, 118(9), 3431–3446. https://doi.org/10.1002/jgrd.50353.

Jobst, A.M., Kingston, D.G., Cullen, N.J. and Sirguey, P. (2017) Combining thin-plate spline interpolation with a lapse rate model to produce daily air temperature estimates in a data-sparse alpine catchment. *International Journal of Climatology*, 37(1), 214–229. https://doi.org/10.1002/joc.4699.

Johannsen, F., Ermida, S., Martins, J., Trigo, I.F., Nogueira, M. and Dutra, E. (2019) Cold bias of ERA5 summertime daily maximum land surface temperature over Iberian Peninsula. *Remote Sensing*, 11, 2570.

Kann, A., Haiden, T. and Wittmann, C. (2011) Combining 2-m temperature nowcasting and short range ensemble forecasting. *Nonlinear Processes in Geophysics*, 18(6), 903–910. https://doi.org/10.5194/npg-18-903-2011.

Kattel, D.B., Yao, T., Yang, K., Tian, L., Yang, G. and Joswiak, D. (2013) Temperature lapse rate in complex mountain terrain on the southern slope of the central Himalayas. *Theoretical and Applied Climatology*, 113(3), 671–682. https://doi.org/10.1007/s00704-012-0816-6.

Li, X., Wang, L., Chen, D., Yang, K., Xue, B. and Sun, L. (2013) Near-surface air temperature lapse rates in the mainland China during 1962–2011. *Journal of Geophysical Research: Atmospheres*, 118(14), 7505–7515. https://doi.org/10.1002/jgrd.50553.

Lute, A.C. and Abatzoglou, J.T. (2021) Best practices for estimating near-surface air temperature lapse rates. *International Journal of Climatology*, 41(S1), E110–E125. https://doi.org/10.1002/joc.6668.

Marshall, S.J., Sharp, M.J., Burgess, D.O. and Anslow, F.S. (2007) Near-surface-temperature lapse rates on the Prince of Wales Icefield, Ellesmere Island, Canada: implications for regional downscaling of temperature. *International Journal of Climatology*, 27(3), 385–398. https://doi.org/10.1002/joc.1396.

Maurer, E.P., Wood, A.W., Adam, J.C., Lettenmaier, D.P. and Nijssen, B. (2002) A long-term hydrologically based dataset of land surface fluxes and states for the conterminous United States. *Journal of Climate*, 15(22), 3237–3251. https://doi.org/10.1175/1520-0442(2002)015<3237:ALTHBD>2.0.CO;2.

Minder, J.R., Mote, P.W. and Lundquist, J.D. (2010) Surface temperature lapse rates over complex terrain: lessons from the Cascade Mountains. *Journal of Geophysical Research*, 115(D14), D14122. https://doi.org/10.1029/2009JD013493.

Mitra, A.K., Momin, I.M., Rajagopal, E.N., Basu, S., Rajeevan, M.N. and Krishnamurti, T.N. (2013) Gridded daily Indian monsoon rainfall for 14 seasons: merged TRMM and IMD gauge analyzed values. *Journal of Earth System Science*, 122(5), 1173–1182. https://doi.org/10.1007/s12040-013-0338-3.

Monestiez, P., Courault, D., Allard, D. and Ruget, F. (2001) Spatial interpolation of air temperature using environmental context: application to a crop model. *Environmental and Ecological Statistics*, 8(4), 297–309. https://doi.org/10.1023/A:1012726317935.

Navarro-Serrano, F., López-Moreno, J.I., Domínguez-Castro, F., Alonso-González, E., Azorin-Molina, C., El-Kenawy, A. and Vicente-Serrano, S.M. (2020) Maximum and minimum air temperature lapse rates in the Andean region of Ecuador and Peru. *International Journal of Climatology*, 40, 6150–6168. https://doi.org/10.1002/joc.6574.

ORNL DAAC. (2017) *Spatial Data Access Tool (SDAT)*. Oak Ridge, TN: ORNL DAAC, https://doi.org/10.3334/ORNLDAAC/1388. Accessed May 25, 2020.

Piani, C., Weedon, G.P., Best, M., Gomes, S.M., Viterbo, P., Hagemann, S. and Haerter, J.O. (2010) Statistical bias correction of global simulated daily precipitation and temperature for the application of hydrological models. *Journal of Hydrology*, 395(3), 199–215. https://doi.org/10.1016/j.jhydrol.2010.10.024.

Podani, J. (2005) Multivariate exploratory analysis of ordinal data in ecology: pitfalls, problems and solutions. *Journal of Vegetation Science*, 16(5), 497–510. https://doi.org/10.1111/j.1654-1103.2005.tb02390.x.

Qin, Y., Ren, G., Zhai, T., Zhang, P. and Wen, K. (2018) A new methodology for estimating the surface temperature lapse rate based on grid data and its application in China. *Remote Sensing*, 10(10), 1617. https://doi.org/10.3390/rs10101617.

Régnière, J. and Sharov, A. (1999) Simulating temperature-dependent ecological processes at the sub-continental scale: male gypsy moth flight phenology as an example. *International Journal of Biometeorology*, 42(3), 146–152. https://doi.org/10.1007/s004840050098.

Ritter, B., Wennrich, V., Medialdea, A., Brill, D., King, G., Schneiderwind, S., Niemann, K., Fernández-Galego, E., Diederich, J., Rolf, C., Bao, R., Melles, M. and Dunai, T.J. (2019) Climatic fluctuations in the hyperarid core of the Atacama Desert during the past 215 ka. *Scientific Reports*, 9(1), 5270. https://doi.org/10.1038/s41598-019-41743-8.

Rolland, C. (2003) Spatial and seasonal variations of air temperature lapse rates in alpine regions. *Journal of Climate*, 16(7), 1032–1046. https://doi.org/10.1175/1520-0442(2003)016<1032:SASVOA>2.0.CO;2.

Romshoo, S.A., Rafiq, M. and Rashid, I. (2018) Spatio-temporal variation of land surface temperature and temperature lapse rate over mountainous Kashmir Himalaya. *Journal of Mountain Science*, 15(3), 563–576. https://doi.org/10.1007/s11629-017-4566-x.

Rozante, J.R., Gutierrez, E.R., de Fernandes, A.A. and Vila, D.A. (2020) Performance of precipitation products obtained from combinations of satellite and surface observations. *International Journal of Remote Sensing*, 41(19), 7585–7604. https://doi.org/10.1080/01431161.2020.1763504.

Rozante, J.R., Moreira, D.S., de Goncalves, L.G.G. and Vila, D.A. (2010) Combining TRMM and surface observations of precipitation: technique and validation over South America. *Weather and Forecasting*, 25(3), 885–894. https://doi.org/10.1175/2010WAF2222325.1.

Satyamurty, P., Nobre, C.A. and Silva Dias, P.L. (1998) South America. In: Karoly, D.J. and Vincent, D.G. (Eds.) *Meteorology of the Southern Hemisphere*. Boston, MA: American Meteorological Society, pp. 119–139.

Scapin, S., Apadula, F., Brunetti, M. and Maugeri, M. (2016) High-resolution temperature fields to evaluate the response of Italian electricity demand to meteorological variables: an example of climate service for the energy sector. *Theoretical and Applied Climatology*, 125(3), 729–742. https://doi.org/10.1007/s00704-015-1536-5.

Schlenker, W. and Roberts, M.J. (2009) Nonlinear temperature effects indicate severe damages to U.S. crop yields under climate change. *Proceedings of the National Academy of Sciences of the United States of America*, 106(37), 15594–15598. https://doi.org/10.1073/pnas.0906865106.

Shea, J.M., Marshall, S.J. and Livingston, J.M. (2004) Glacier distributions and climate in the Canadian Rockies. *Arctic, Antarctic, and Alpine Research*, 36(2), 272–279. https://doi.org/10.1657/1523-0430(2004)036[0272:GDACIT]2.0.CO;2.

Shen, Y.-J., Shen, Y., Goetz, J. and Brenning, A. (2016) Spatial-temporal variation of near-surface temperature lapse rates over the Tianshan Mountains, central Asia. *Journal of Geophysical Research: Atmospheres*, 121(23), 14006–14017. https://doi.org/10.1002/2016JD025711.

Shuai Han, C.S. and Shuai Han, C.S. (2019) Development and evaluation of hourly and kilometer resolution retrospective and real-time surface meteorological blended forcing dataset (SMBFD) in China. *Journal of Meteorological Research*, 33, 1168–1181. https://doi.org/10.1007/s13351-019-9042-9.

Tarek, M., Brissette, F.P. and Arsenault, R. (2020) Evaluation of the ERA5 reanalysis as a potential reference dataset for hydrological modelling over North America. *Hydrology and Earth System Sciences*, 24(5), 2527–2544. https://doi.org/10.5194/hess-24-2527-2020.

Tetzner, D., Thomas, E. and Allen, C. (2019) A validation of ERA5 reanalysis data in the southern Antarctic Peninsula—Ellsworth land region, and its implications for ice core studies. *Geosciences*, 9(7), 289. https://doi.org/10.3390/geosciences9070289.

Tobin, C., Nicotina, L., Parlange, M.B., Berne, A. and Rinaldo, A. (2011) Improved interpolation of meteorological forcings for hydrologic applications in a Swiss Alpine region. *Journal of Hydrology*, 401(1), 77–89. https://doi.org/10.1016/j.jhydrol.2011.02.010.

Tukey, J.W. (1977) *Exploratory Data Analysis*. Reading, MA: Addison-Wesley.

Vera, C., Baez, J., Douglas, M., Emmanuel, C.B., Marengo, J., Meitin, J., Nicolini, M., Nogues-Paegle, J., Paegle, J., Penalba, O., Salio, P., Saulo, C., Silva Dias, M.A., Dias, P.S. and Zipser, E. (2006) The South American low-level jet experiment. *Bulletin of the American Meteorological Society*, 87(1), 63–78. https://doi.org/10.1175/BAMS-87-1-63.

Vila, D.A., de Goncalves, L.G.G., Toll, D.L. and Rozante, J.R. (2009) Statistical evaluation of combined daily gauge observations and rainfall satellite estimates over continental South America. *Journal of Hydrometeorology*, 10(2), 533–543. https://doi.org/10.1175/2008JHM1048.1.

Vizuete, W., Junquera, V., McDonald-Buller, E., McGaughey, G., Yarwood, G. and Allen, D. (2002) Effects of temperature and land use on predictions of biogenic emissions in eastern Texas, USA. *Atmospheric Environment*, 36(20), 3321–3337. https://doi.org/10.1016/S1352-2310(02)00272-8.

Wang, Y., Wang, L., Li, X. and Chen, D. (2018) Temporal and spatial changes in estimated near-surface air temperature lapse rates on Tibetan Plateau. *International Journal of Climatology*, 38(7), 2907–2921. https://doi.org/10.1002/joc.5471.

World Meteorological Organization (WMO). (2010) *Guide to the Global Observing System*. Geneva: WMO.

Xu, C.-D., Wang, J.-F., Hu, M.-G. and Li, Q.-X. (2014) Estimation of uncertainty in temperature observations made at meteorological stations using a probabilistic spatiotemporal approach. *Journal of Applied Meteorology and Climatology*, 53(6), 1538–1546. https://doi.org/10.1175/JAMC-D-13-0179.1.

Zhang, Y., Cai, C., Chen, B. and Dai, W. (2019) Consistency evaluation of precipitable water vapor derived from ERA5, ERA-Interim, GNSS, and radiosondes over China. *Radio Science*, 54(7), 561–571. https://doi.org/10.1029/2018RS006789.

Zhao, C., Liu, B., Piao, S., Wang, X., Lobell, D.B., Huang, Y., Huang, M., Yao, Y., Bassu, S., Ciais, P., Durand, J.-L., Elliott, J., Ewert, F., Janssens, I.A., Li, T., Lin, E., Liu, Q., Martre, P., Müller, C., Peng, S., Peñuelas, J., Ruane, A.C., Wallach, D., Wang, T., Wu, D., Liu, Z., Zhu, Y., Zhu, Z. and Asseng, S. (2017) Temperature increase reduces global yields of major crops in four independent estimates. *Proceedings of the National Academy of Sciences of the United States of America*, 114(35), 9326–9331. https://doi.org/10.1073/pnas.1701762114.

How to cite this article: Rozante, J. R., Ramirez, E., & Fernandes, A. d. A. (2021). A newly developed South American Mapping of Temperature with estimated lapse rate corrections. *International Journal of Climatology*, 1–18. https://doi.org/10.1002/joc.7356